Micro-nanoarchitectonics of Electroless Cu/Ni Composite Materials Based on Wood *via* Heat Treatment

Yanfei Pan,[a,b,1,*] Mayin Dai,[a,b,1] Xin Zheng,[a, b,1] Lei Yun,[a, b,1] Fengqi Qiu,[a,b,1] Dongbo Yang,[a,b] Caiyi Deng,[a,b] Qiang Guo,[a,b] and Jintian Huang [a,b,*]

This research aims to optimize the comprehensive performance of wood-based electromagnetic shielding interference (EMI) materials and master the effect of heat treatment on its coating density, interfacial morphology, conductivity, and hydrophobic and electromagnetic shielding. The results showed that the surface roughness of composite coatings was 11.0 μm when the wood was conducted *via* electroless two deposition Cu and one Ni and the heat treatment temperature was 150 °C. The composite coating's surface gradually became more uniform with increasing temperature. The coating's thickness *via* 120 °C heat treatment was 97.5 μm. Energy Dispersive Spectroscopy (EDS) spectra verified the existence of Cu and Ni particles. The heat treatment had an obvious influence on conductivity of composite materials and the pore network structure. The contact angle of composite materials reached 119°. The average electromagnetic shielding efficiency *via* 180 °C heat treatment was up to 91.4 dB in the frequency ranging from 300 to 3.0 GHz, which verified that the composite materials can shield 99.99% of the incident electromagnetic wave energy. The conductivity gradient structure can realize multi-dielectric interface loss and multiple reflection loss.

DOI: 10.15376/biores.17.4.6718-6739

Keywords: Wood; Electroless Cu-Ni; Conductivity; Hydrophobicity; Electromagnetic shielding

Contact information: a: College of Material Science and Art Design, Inner Mongolia Agricultural University, Hohhot, China, 010018; b: Inner Mongolia Key Laboratory for Sand Shrubs Fibrosis and Energy Development and Utilization; 1: These authors contributed equally to this work;
** Corresponding authors: panyanfeiz@imau.edu.cn; jintian_h@imau.edu.cn*

INTRODUCTION

Electromagnetic pollution has become an inevitable social problem as communication technologies represented by emerging 5G wireless systems and modern electronics flourish (Chen *et al*. 2013; Meng *et al*. 2018; Srivastava and Manna 2022; Xiong *et al*. 2022). The elimination of harmful electromagnetic waves is necessary for the protection of electronic communication equipment and the maintenance of healthy human living circumstances (Thomassin *et al*. 2013; Abbasi *et al*. 2019; Wang *et al*. 2019). The matrix of commonly used electromagnetic shielding materials is mostly non-renewable and not easy to degrade; thus, large-scale use will bring environmental problems (Hu *et al*. 2021). Therefore, it will be an inevitable trend to prepare shielding materials based on environment-friendly materials with rich resources that are renewable and degradable (Zheng *et al*. 2020; Xiong *et al*. 2022).

In recent years, many researchers have focused on the preparation of lightweight and efficient biomass-based EMI shielding materials that take advantage of the green and sustainable nature of biomass resources (Qi *et al*. 2021; Jia *et al*. 2022). For example, Shen

et al. prepared epoxy (EP)/carbon composites by filling epoxy into carbonized wood. The EP/ C-1200 composite exhibited a maximum SE value of 27.8 dB at a thickness of 3 mm (Shen *et al*. 2019). Liang *et al*. (2020) demonstrated an MXene aerogel/wood PC composite with excellent electrical conductivity, achieving a SE value of 69.4 dB at 3 mm. Gan *et al*. (2020) prepared conductive wood by delignification and chemical vapor deposition and obtained 58 decibels of SE at 3.5 cm. Generally, EMI shielding performance is contributed by two parts: reflection and absorption. Reflection is related to the dielectric properties of the material, while absorption is related to the multiple loss characteristics (Lou *et al*. 2021; Yu *et al*. 2022). Therefore, in order to further optimize the shielding performance of wood-based materials and improve the total SE of wood-based materials, heat treatment of wood-based materials is a useful method.

As a green physical modification method, wood heat treatment can increase the dimensional stability and biological durability of wood, which is an effective technical means to improve the utilization of wood resources (Fang 2019). During heat treatment, the components of wood are degraded. Compared with untreated wood, the compressive strength of heat-treated wood often shows a certain degree of improvement. After high temperature heat treatment, the moisture absorption, degradation resistance and dimensional stability of wood were improved (Ma 2019; Lin 2021; Yan 2021; Yu 2021). Moreover, after high-temperature heat treatment, the hydrophilic groups in the wood decrease and the surface wettability of the wood decreases (Hao *et al*. 2021). As with all solids, most of the properties of electroless Ni and Cu coatings are temperature-dependent. The thermal expansion coefficient affects the internal stress and bonding strength of electroless Ni and Cu coatings without high temperature heat treatment, which are thermodynamically metastable and tend to change from amorphous or microcrystalline state to crystalline state. Under certain conditions, when the composite coatings are heat-treated, atoms in the coatings will have mutual diffusion, resulting in recrystallization of amorphous or microcrystalline structure, and the formation of metallic Ni and intermetallic compounds, such as Ni_2P, Ni_3P, and Ni_5P_2 (Pan *et al*. 2020). Generally speaking, heat treatment will change the coating's structure, and the structural change will affect the coating's performance. However, there have been few reports on the relationship between heat treatment and electromagnetic shielding efficiency of Ni-Cu-P ternary wood-based composites.

In this study, the relationship between electromagnetic shielding effectiveness and heat treatment temperature of wood-based composite materials *via* electroless Cu and electroless Ni was analyzed. After the optimal heat treatment temperature, the electromagnetic shielding effectiveness of the composite material prepared by us can reach 90.40 dB in the L-band, which has a good application prospect in the aerospace and military fields.

EXPERIMENTAL

Reagents and Materials

Copper sulfate pentahydrate ($CuSO_4·5H_2O$), Seignette salt ($NaKC_4H_4O_6·4H_2O$), ethylenediaminetetraacetic acid disodium salt (EDTA-2Na), potassium ferrocyanide ($K_4Fe(CN)_6·3H_2O$), formaldehyde, NaOH, nickel sulfate hexahydrate ($NiSO_4·6H_2O$), sodium hypophosphite ($NaH_2PO_2·H_2O$), sodium citrate ($Na_3C_6H_5O_7·H_2O$), thiourea (CH_4N_2S), borohydride sodium ($NaBH_4$), hydrochloric acid (HCl), and ammonia water

($NH_3 \cdot H_2O$) all were analytically pure and purchased from Tianjin Beilian Fine Chemicals Development Co., Ltd. The base fluid was deionized water.

Poplar was selected as the base material, which was collected from Tumotezuoqi, Hohhot, China, with a tree age of 3 to 5 years. Poplar wood without growth defects was cut into round chips 9 cm in diameter. Thickness was 0.37 ±0.05 mm. The moisture content was about 11.2%.

Experimental Design

Six temperature gradients were designed. After electroless Cu and electroless Ni treatment, the wood was heat treated at 25 ℃, 100 ℃, 120 ℃, 150 ℃, 180 ℃, and 200 ℃. The experimental design is shown in Table 1. Specimens were labeled based on the types of electroless treatment. For example, when the wood was modified *via* two electroless Cu treatments and then one electroless Ni treatment, the sample was marked as 2CulNi.

Table 1. Experimental Design

Type	Temperature (°C)					
	25	100	120	150	180	200
Electroless Cu-Ni	1	2	3	4	5	6

Preparation of Specimens

Substrate preparation

Poplar chips without surface defects were screened from poplar wood. The poplar chips were rubbed with 600 mesh sandpaper to make them smooth. Then, the wood chips were cut into round sheets with a diameter of 9 cm, and then boiled in a water bath at 100 ℃ to remove the impurities inside the poplar.

Fig. 1. Schematic diagram of sample preparation

Electroless Cu

First, the specimen was placed in the activation solution A ($CuSO_4 \cdot 5H_2O$ 15 g/L, HCl 12 mL/L) and activated for 15 min. Then it was removed and placed into the activation solution B ($NaBH_4$ 15 g/L, NaOH 15 g/L) to activate for 90 s. $CuSO_4 \cdot 5H_2O$ (53 g/L), $NaKC_4H_4O_6 \cdot 4H_2O$ (13 g/L), EDTA-2Na (27 g/L), $K_4Fe(CN)_6 \cdot 3H_2O$ (1.3 g/L), and HCHO (70 mL/L) were added to the beaker containing 150 mL distilled water. Electroless Cu was carried out in the prepared plating solution at pH =11.8 (it was adjusted with 25% NaOH) and a temperature of 60 °C. The electroless Cu was carried out, as shown in Fig. 2.

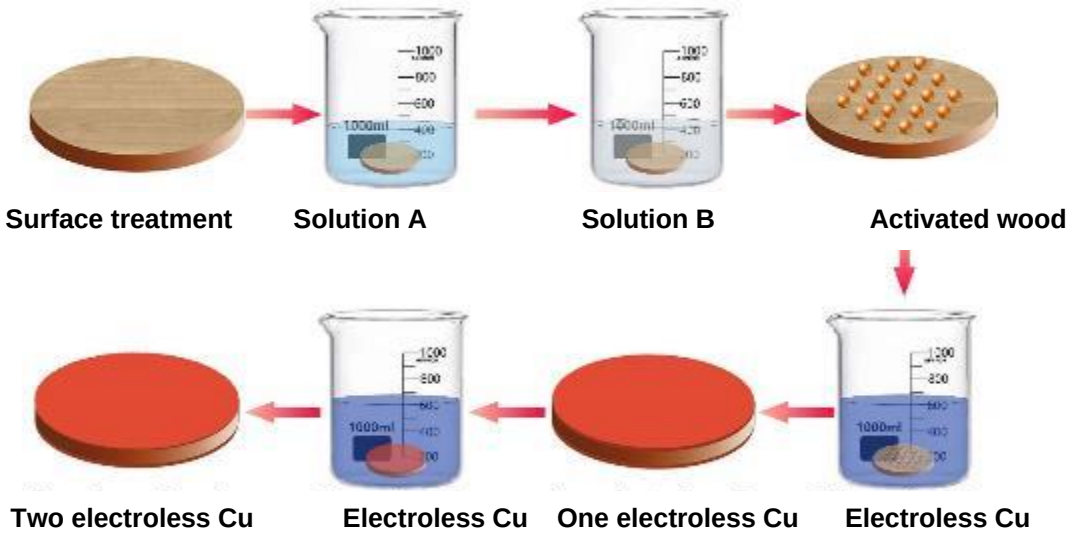

Fig. 2. Schematic diagram of electroless Cu on wood surface

Electroless Ni

Two electroless Cu samples were activated in electroless Ni activator A ($NiSO_4 \cdot 6H_2O$ 15 g/L, HCl 12 mL/L) for 15 min. The samples were taken out and exposed to the activation solution B ($NaBH_4$ 15 g/L, NaOH 15 g/L) for 90 s. $NiSO_4 \cdot 6H_2O$ (33 g/L), $NaH_2PO_2 \cdot 2H_2O$ (28 g/L), $Na_3C_6H_5O_7 \cdot H_2O$ (30 g/L), and CH_4N_2S (10 mg/L) were added to the beaker containing 350 mL distilled water. Electroless Ni coating was carried out in the prepared plating solution at pH = 9 (adjusted with ammonia) and a temperature of 60 °C. The electroless Ni was carried out, as shown in Fig. 3.

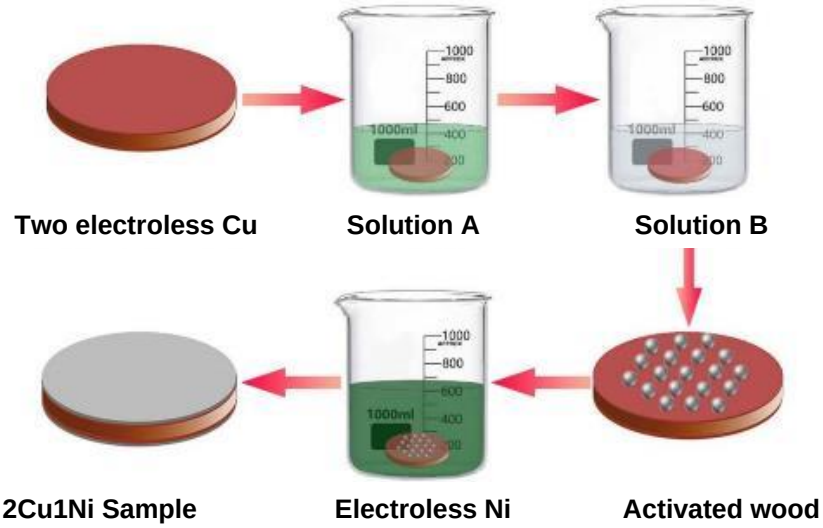

Fig. 3. Schematic diagram of electroless Ni on wood surface

Heat treatment of 2Cu1Ni sample

The samples were put into a furnace, and the samples were clamped by fixtures. Six temperature gradients were designed. The wood was treated by electroless Cu-Ni, and then heat treated at 25 °C, 100 °C, 120 °C, 150 °C, 180 °C, and 200 °C, in turn, and then the performance was tested (Fig. 4).

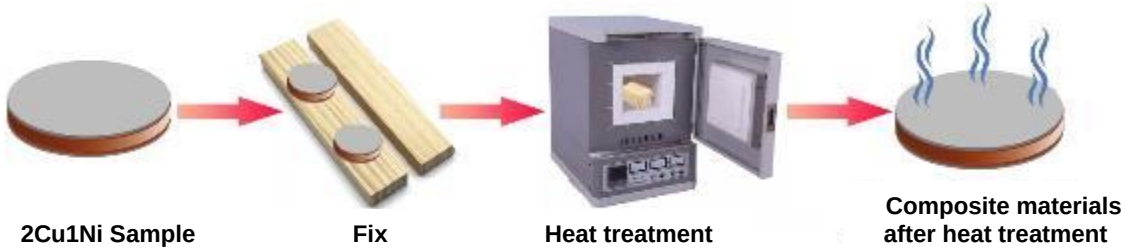

Fig. 4. Schematic diagram of heat-treated wood-based composite

Testing Instrument and Operation Procedure

VK-X160 laser scanning confocal microscope test

A laser scanning confocal microscope (VK-X160, Keyence, Osaka, Japan) was used for observing the overall surface morphology of composite materials and the roughness of coating surface. The specific operation method is to open the laser scanning confocal microscope first, then open the computer and observation software in turn, and place each group of test samples in the center of the sample table. The largest objective was chosen 20 times the size of the observation.

RTS-8 four-probe

A four-probe tester (RST-8, Guangzhou Four-probe Technology Co., Ltd., Guangzhou, China) was used for testing the electrical conductivity of composites. The specific test method is to measure the samples at five different positions along the horizontal and grain lines, and take five different points at each position to test the resistance and take the average value.

Scanning electron microscopy (SEM)

A scanning electron microscope (Phenom, Thermo Fisher Scientific, Waltham, MA, USA) was employed to characterize the microstructure of composite materials.

Hydrophobic performance

A contact angle meter (JY-PHa, Chengde Youte Instrument Manufacturing Co., Ltd., Chengde, China) was used to characterize the hydrophobicity of composite materials. The specific test procedure is to measure a composite sample at five different positions after 20 s of dripping, select two similar values from five values, and take the average.

DR-S02A electromagnetic shielding effectiveness

The DR-S02A shielding effectiveness test device (Beijing DingrongShichuang Technology Co., Ltd., Beijing, China) was used to characterize the electromagnetic shielding performance of the composite material. The test frequency range is between 0.3×10^{-3} and 3.0×10^{3} MHz. The composites were tested according to the ASTM 4935 (2010) international standard test. The sample thickness was ≤ 10 mm. The error was from +0.5 dB to -0.5 dB, and the maximum VSWR (voltage standing wave ratio) was less than 1.2. The insertion loss (IL) was < 0.5 dB.

According to Schelkunoffs theory (Pan *et al*. 2022), the detailed formulas are as follows:

$$\mathrm{SE}_T(\mathrm{dB}) = SE_R + SE_A + SE_M \quad (1)$$

$$\mathrm{SE}_R(\mathrm{dB}) = -10\log(1 - S_{11}^2) \quad (2)$$

$$\mathrm{SE}_A(\mathrm{dB}) = -10\log[(S_{21}^2/(1 - S_{11}^2)] \quad (3)$$

In these equations, S_{11} and S_{21} are the measured scattering parameters. When the SE_T is more than 15 dB, SE_M can be ignored. Formula 1 can be simplified as:

$$\mathrm{SE}_A(\mathrm{dB}) = SE_R + SE_A \quad (4)$$

RESULTS AND DISCUSSION

Heat Treatment Coatings Morphology

Figure 5 shows the surface morphology of wood without superheat treatment. Comparing Fig. 5a with 5b (3D image), it could be clearly observed that copper and nickel were deposited on the composite material surface *via* electroless Cu-Ni, which partially covered the whole area, and the morphology of wood grain pores disappeared.

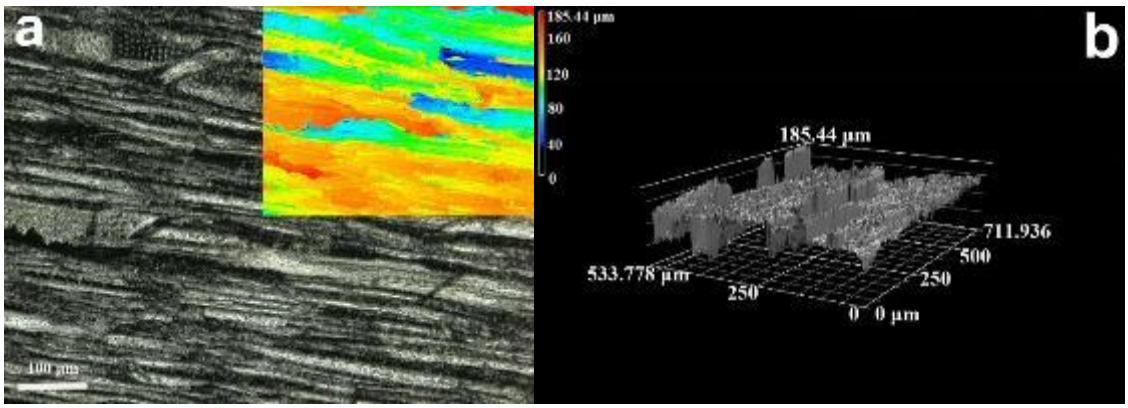

Fig. 5. The wood surface laser microscope morphology 200× (a: Surface morphology; inset shows depth map; b: 3D image)

Figure 6 showed that the surface morphology of the wood was partially uneven. The maximum surface roughness of metal coatings on wood surface was 33.8 µm (Table 2). The 3D images after heat treatment (Fig. 7) showed that with the increase of heat treatment temperature, the surface roughness of the bonded metal coatings could be as low as 11.0 µm (Table 2).

The rate of metal ion deposition on smooth wood surface was affected by the catalysis of matrix and deposition (Pan *et al*. 2022). The metal coatings on the wood surface were gradually transformed with compact deposition with increasing temperature, which further verified that the heat treatment could accelerate metal Cu and Ni particle rearrangement and optimized the surface structure.

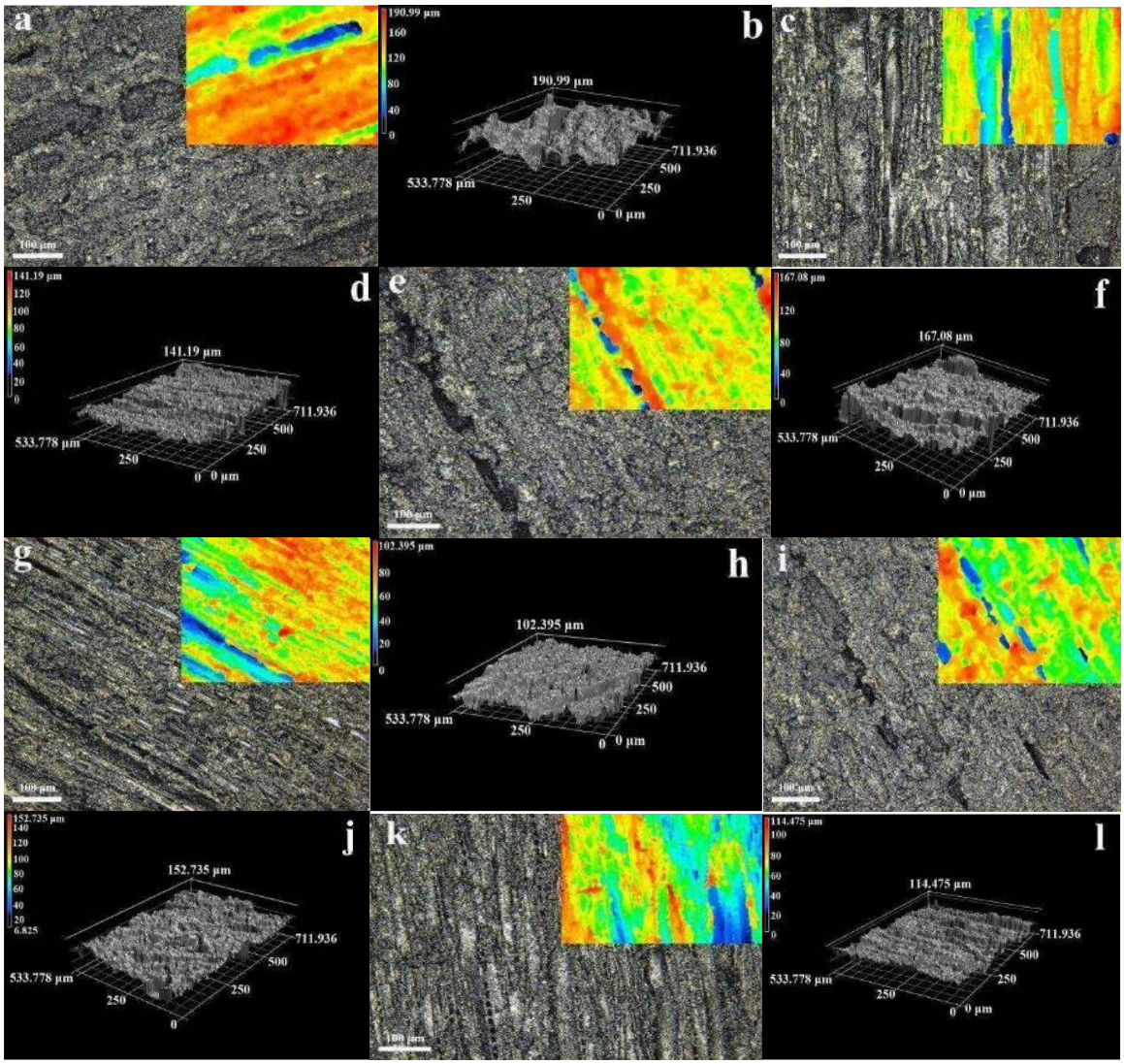

Fig. 6. The laser microscope morphology of 2Cu1Ni electroless plated wood before heat treatment is 200 × (a-k temperature treatment is 25 °C, 100 °C, 120 °C, 150 °C, 180 °C, 200 °C ; embedded well depth map ; the processing temperatures of 3D images from B to l are 25 °C, 100 °C, 120 °C, 150 °C, 180 °C and 200 °C, respectively

Table 2. Surface Roughness

Temperature (°C)	Before Heat Treatment (μm)	After Heat Treatment (μm)
25	19.7	19.7
100	33.8	14.3
120	18.3	13.9
150	21.8	11.0
180	25.4	12.7
200	21.7	11.7

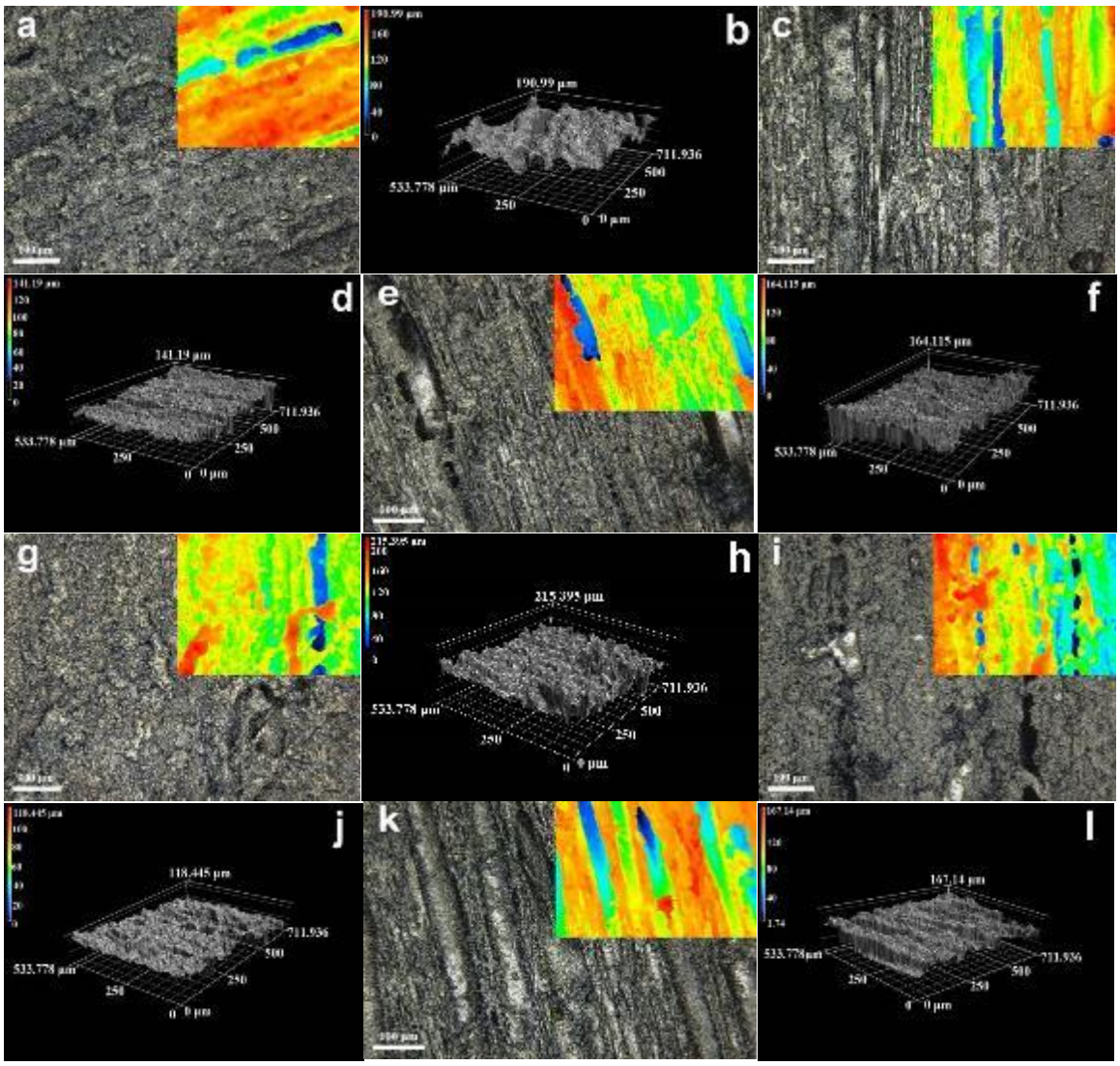

Fig. 7. The laser microscope morphology of 2Cu1Ni electroless plated wood after heat treatment is 200 × (a-k temperature treatment is 25 °C, 100 °C, 120 °C, 150 °C, 180 °C, 200 °C ; embedded well depth map ; the processing temperatures of 3D images from B to l are 25 °C, 100 °C, 120 °C, 150 °C, 180 °C, and 200 °C, respectively

Surface Morphology

Figure 8 shows the SEM morphology of wood surface *via* electroless Cu-Ni. After electroless Cu-Ni and different heat treatments, the distribution of metal coating on the wood surface tended to be flat. There were obvious pore structures on the coating's surface (Fig. 8a), and there were local agglomerations. The pore structures were obvious, and the number of pore structures clearly increased with increase in temperature (Fig. 8b). More pore structures resulted in smaller grains (Fig. 8f). The pore morphology of electroless Cu-Ni composite coatings were ideal when the heat treatment temperature was 180 ℃.

Figures 9 and 10 show the area scanning and local point energy spectra of composite coatings of different heat treatments. To verify the uniform dispersion of metal particles in the coatings after heat treatment, two different areas were selected in the composite coatings scanning image. The composite coatings mainly included the five

elements Ni, Cu, P, C, and O. The main elements were Ni and Cu, which further verified the results of laser confocal microscopy. At the same time, surface scanning and local point energy spectra showed that the Ni and Cu particles were tightly embedded together. Therefore, when the heat treatment temperature was 120 ℃, the number of pore structure was less, indicating that the morphology of electroless Cu-Ni composite coatings on the wood surface were ideal.

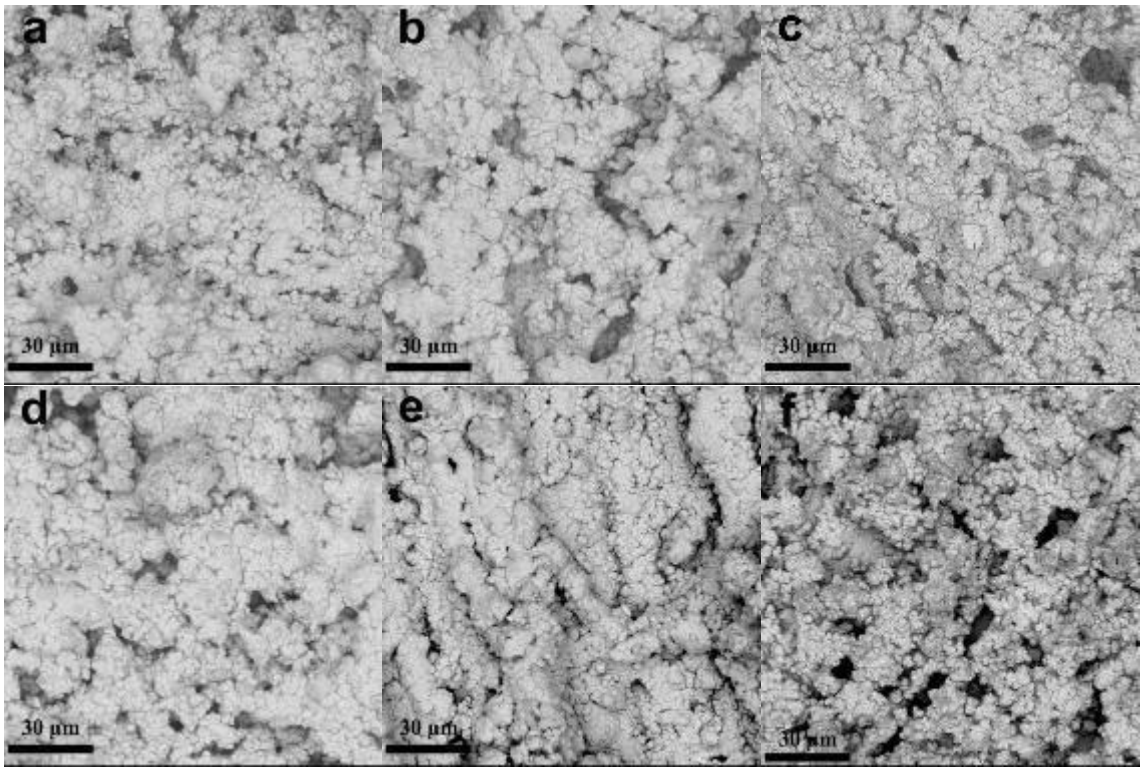

Fig. 8. Electroless 2Cu1Ni wood surface morphology after heat treatment (a, b, c, d, e, and f)

Cross-section Morphology of Composites

Figure 11 shows the cross-section morphology *via* electroless Cu-Ni with different heat treatments. It shows that the coating's thickness would also change with the increase of heat treatment temperature, showing a trend of first increase and then decrease. Cu and Ni particles were fully embedded in the pores of wood, and the thickness of metal coatings on the wood surface reached 97.48 μm when the electroless temperature reached 120 °C (Table 3). The appearance of the interfacial morphology of the composite material verified that the surface and interface morphology of the composite coatings were better at 120 °C. The bright white wood in the cross-sectional morphology showed that the metal Cu and Ni particles penetrated into the wood pores, which was conducive to the formation of dense and high-strength composites. The cross-sectional morphology showed that a bright white area in the wood pores, which further illustrated that the metal Cu and Ni particles entered the wood pores. The heat treatment could accelerate the rearrangement of Cu and Ni metal particles rearrangement, and an ideal pore structure could be obtained. A conclusion could be drawn that the Cu and Ni nanoparticles could enter the pore structure of wood, so the intrinsic permeable channel design of wood where the conductive network structure was constructed, which could realize various reflection losses of electromagnetic waves.

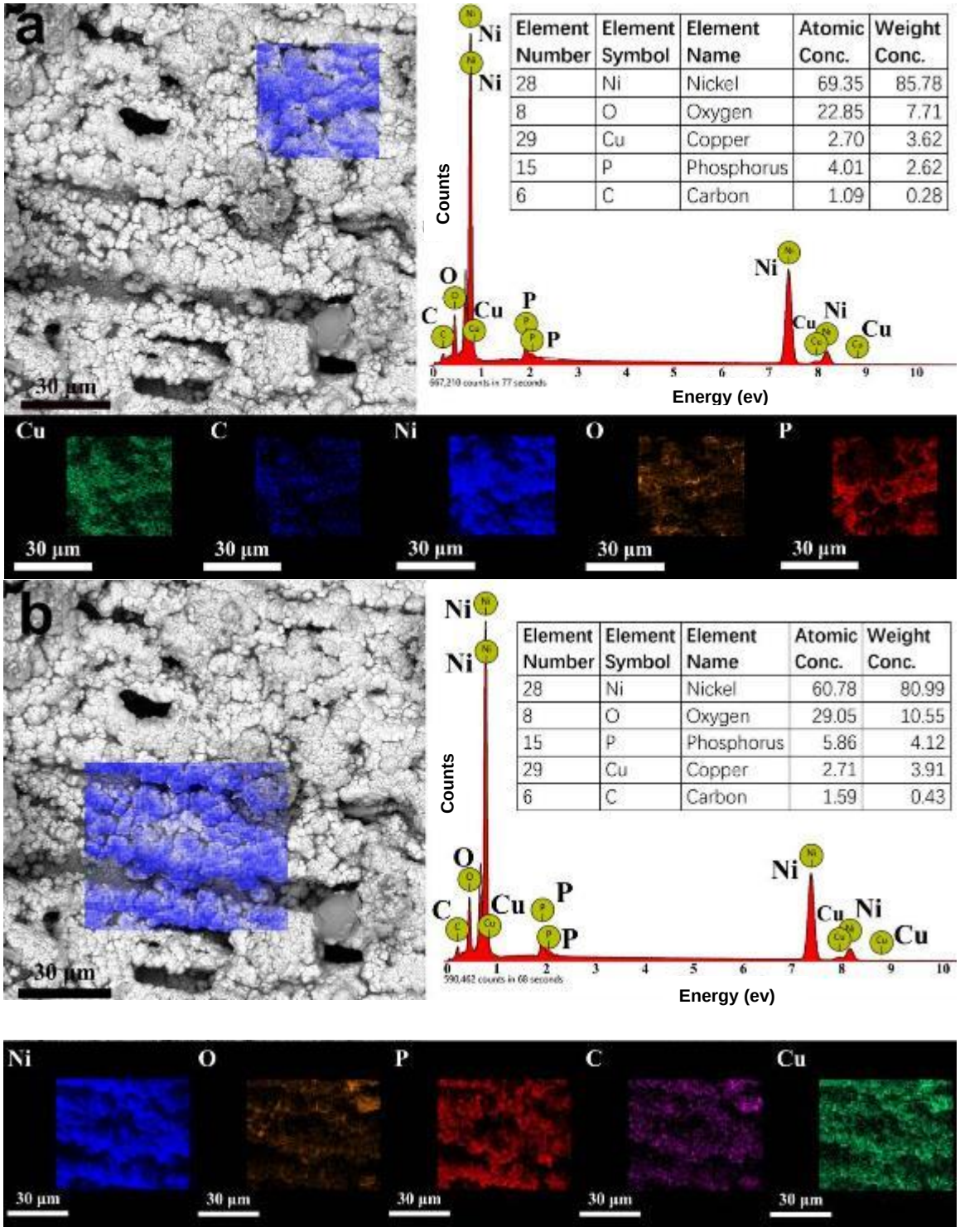

Element Number	Element Symbol	Element Name	Atomic Conc.	Weight Conc.
28	Ni	Nickel	69.35	85.78
8	O	Oxygen	22.85	7.71
29	Cu	Copper	2.70	3.62
15	P	Phosphorus	4.01	2.62
6	C	Carbon	1.09	0.28

Element Number	Element Symbol	Element Name	Atomic Conc.	Weight Conc.
28	Ni	Nickel	60.78	80.99
8	O	Oxygen	29.05	10.55
15	P	Phosphorus	5.86	4.12
29	Cu	Copper	2.71	3.91
6	C	Carbon	1.59	0.43

Fig. 9. Energy dispersive spectra of 150 °C heat-treated by electroless 2Cu1Ni (a and b)

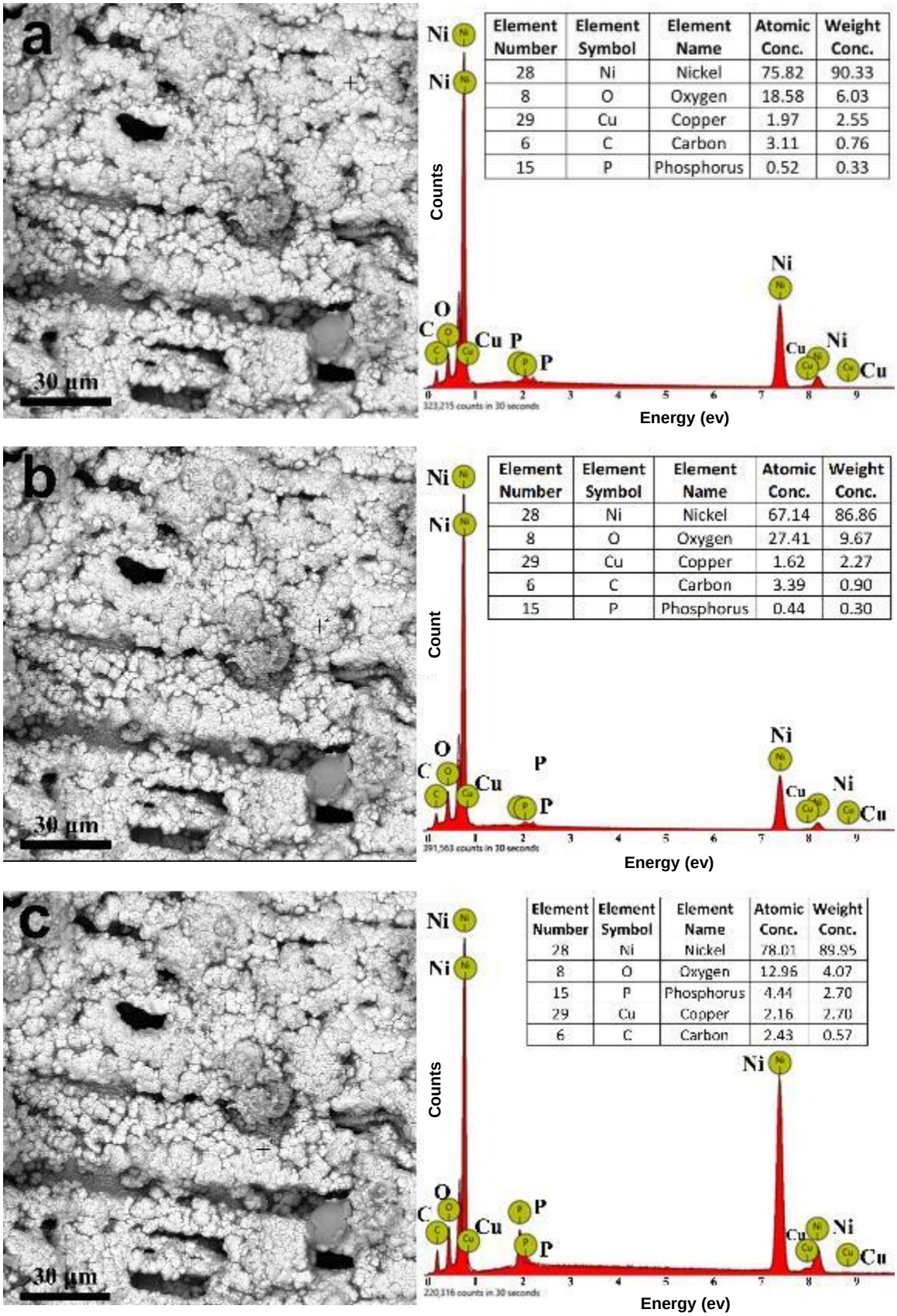

Element Number	Element Symbol	Element Name	Atomic Conc.	Weight Conc.
28	Ni	Nickel	75.82	90.33
8	O	Oxygen	18.58	6.03
29	Cu	Copper	1.97	2.55
6	C	Carbon	3.11	0.76
15	P	Phosphorus	0.52	0.33

Element Number	Element Symbol	Element Name	Atomic Conc.	Weight Conc.
28	Ni	Nickel	67.14	86.86
8	O	Oxygen	27.41	9.67
29	Cu	Copper	1.62	2.27
6	C	Carbon	3.39	0.90
15	P	Phosphorus	0.44	0.30

Element Number	Element Symbol	Element Name	Atomic Conc.	Weight Conc.
28	Ni	Nickel	78.01	89.95
8	O	Oxygen	12.96	4.07
15	P	Phosphorus	4.44	2.70
29	Cu	Copper	2.16	2.70
6	C	Carbon	2.43	0.57

Fig. 10. EDS spectra of Electroless 2Cu1Ni (a, b, and c)

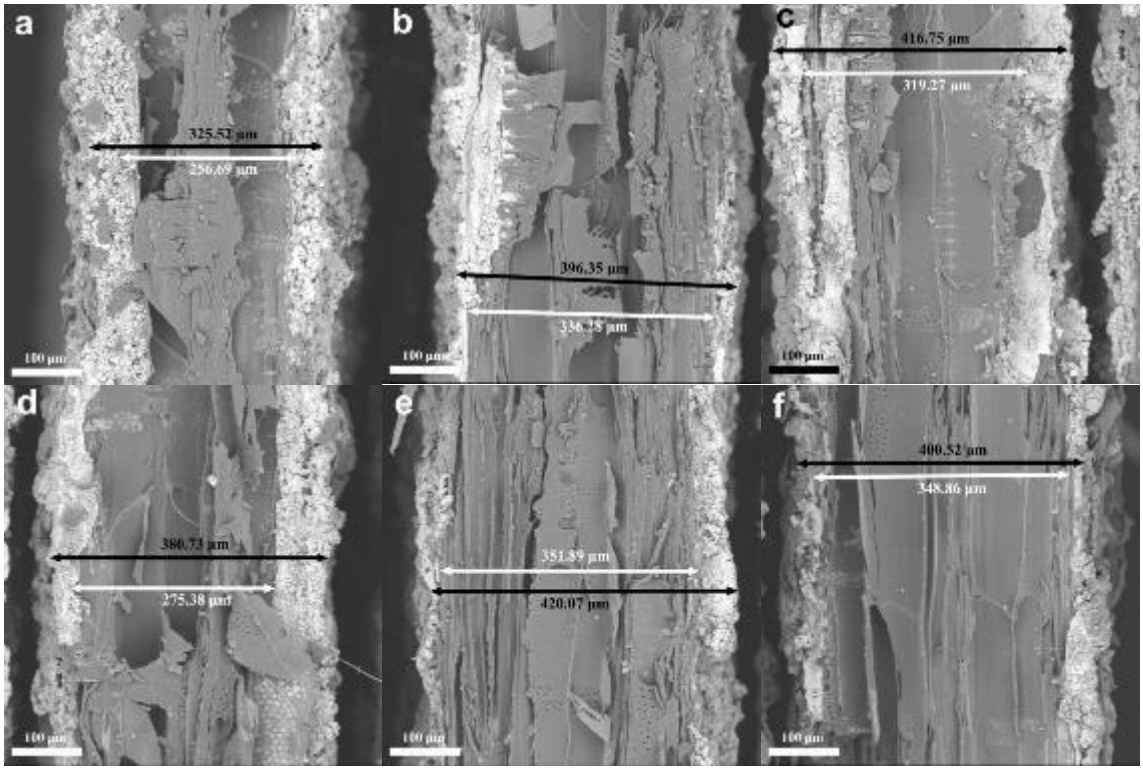

Fig. 11. Cross-section morphology after heat treatment (a: 25 °C, b: 100 °C, c: 120 °C, d: 150 °C, e: 180 °C, and f: 200 °C)

Table 3. Thickness of Coating Cross-section after Heat Treatment

Temperature (°C)	Thickness (μm)
25	70.83
100	46.87
120	97.48
150	49.48
180	68.18
200	40.63

Conductivity

Figure 12 shows the relationship between heat treatment and the conductivity of coatings. Figure 12a shows that the conductivity of 2Cu1Ni electroless composite decreased first and then it tended to be stable. The electrical conductivity decreased from 25 °C to 100 °C, then tended to be stable. Figure 12b shows the conductivity of electroless 2Cu1Ni composite increased at 100 °C, 150 °C, and 180 °C, while the conductivity decreased at 120 °C and 200 °C. It could be concluded from Fig. 12 that the electrical conductivity of the coatings on the composite surface varied greatly *via* heat treatment. The main reason was the acceleration of rearrangement and recrystallization of Cu and Ni in process of heat treatment. The Cu and Ni particles rapidly accumulated on the wood surface. The metal coatings covered the whole wood surface and the difference of materials, the uniformity and thickness of the composite coatings rapidly increased, which made the electrical conductivity of the wood composite increase.

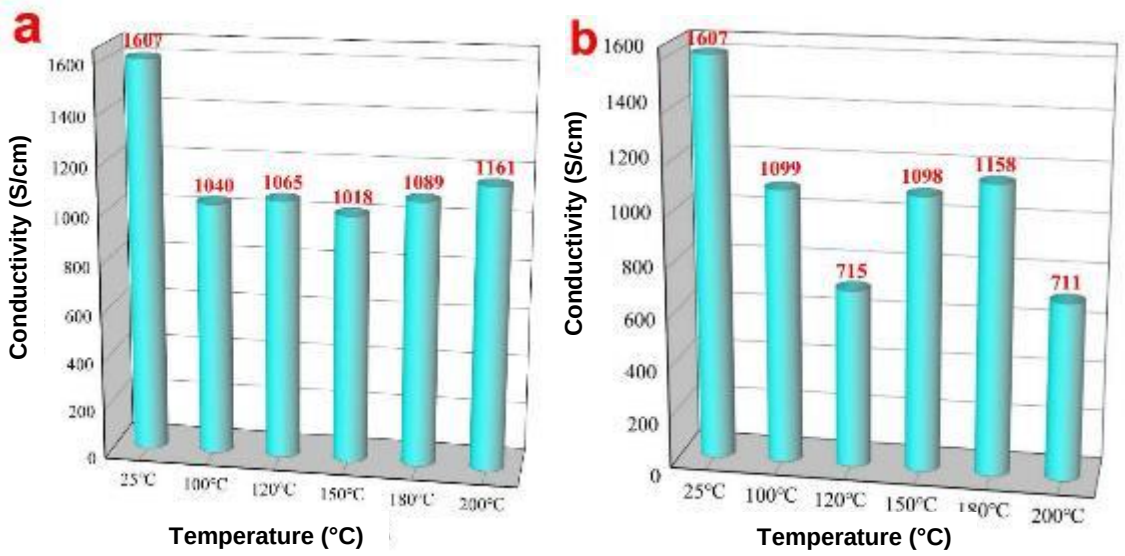

Fig. 12. Relationship between heat treatment temperature and conductivity (a: without heat treatment, b: heat treatment)

Figure 12 shows the electrical conductivity of the wood surface increased *via* heat treatment. With the increase of temperature, the rearrangement and recrystallization of Cu and Ni accelerated, and the wood surface would form dense, uniform, and conductive network structure composites.

Hydrophobic Performance

Figure 13 illustrates the surface hydrophobicity of the materials treated with different heat treatment. The heat treatment temperatures were 25 °C, 100 °C, 120 °C, 150 °C, 180 °C, and 200 °C, and the contact angles resulting from electroless 2Cu1Ni with different temperature gradients were 108.8, 119.1, 108.5, 115.8, 100.5, and 104.7, respectively (Table 4). When the temperature of electroless 2Cu1Ni composites reached 100 °C, the contact angle was 119.1°. This result further verified the correctness of the SEM analysis conclusion. Compared with the hydrophobic treatment method mentioned in the literature (Xiao *et al*. 2020), the composite coatings formed by heat treatment on the wood surface could improve the hydrophobic properties of the material, which demonstrated that the metal Cu and Ni on the wood surface were tightly embedded together to form a dense composite coating. This happened because the rearrangement and recrystallization of Cu and Ni were accelerated, and the Cu and Ni coatings were tightly embedded together. The roughness decreased gradually, the surface coating smoothness tended to become more uniform, and the particles were closely combined. Therefore, the metal coating structure on the wood surface was relatively dense, and the hydrophobic property of the composite was better. The hydrophobic property of the composite at 100 °C was better than at 200 °C. The possible reason was that the thickness of the composite coating increased gradually with the increase of temperature on the wood surface, resulting in the difference in the local surface roughness (Sun *et al*. 2015).

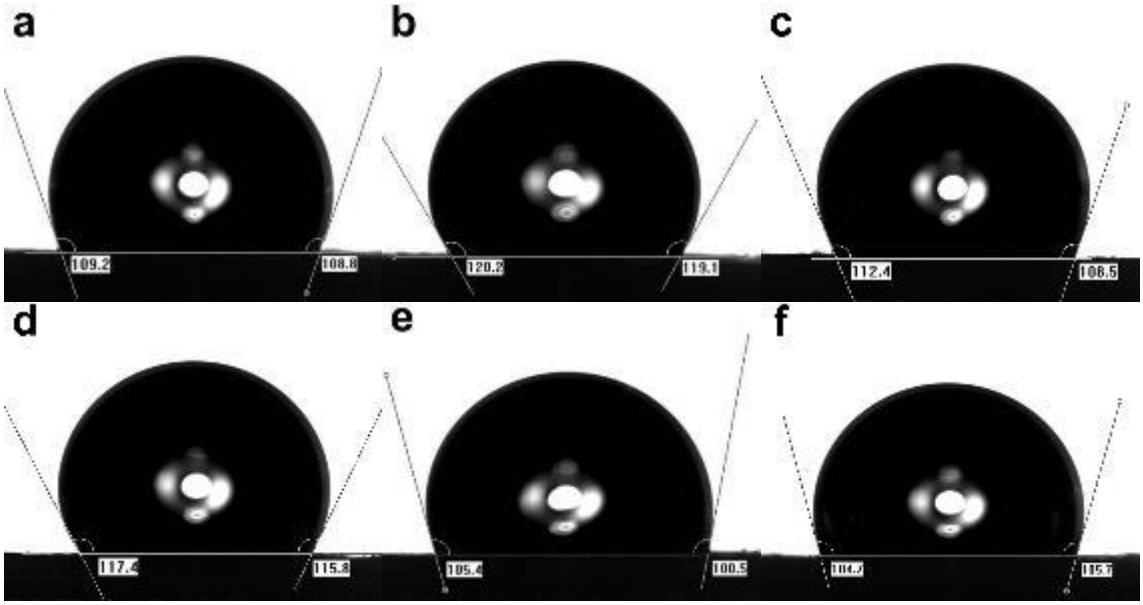

Fig. 13. Hydrophobic properties of electroless 2Cu1Ni after heat treatment (a: 25 °C, b: 100 °C, c: 120 °C, d: 150 °C, e: 180 °C, f: 200 °C)

Table 4. Contact Angles at Different Temperatures After Heat Treatment

Temperature (°C)	Contact Angle (°)
25	108.8
100	119.1
120	108.5
150	115.8
180	100.5
200	104.7

Electromagnetic Shielding Effectiveness

Figures 14 and 15 show the electromagnetic shielding effectiveness curves of the composites, which were wood-based composites formed *via* electroless 2Cu1Ni on the wood surface and heat treatment. The average electromagnetic shielding efficiency reached 91.40 dB, ranging from 300 KHz to 3.0 GHz (Table 5), which verified that the composite material could efficiently shield the incident electromagnetic wave.

The absorption spectra showed that the composites *via* electroless 2Cu1Ni treated at 100 °C had stronger electromagnetic wave absorption capacity. The reflection spectra showed that the electroless 2CuNi treated at 120 °C had stronger reflection on electromagnetic waves in the frequency ranging from 2.5 to 3.0 GHz (Figs. 15a and 15b). Due to good impedance matching, the incident electromagnetic wave could easily penetrate the interior of the composite coatings, and a few electromagnetic waves could be reflected on the surface of the composite coating. The porous structure of composite coating on wood surface was beneficial to electromagnetic wave absorption. The absorption coatings with positive conductivity gradient and negative magnetic (Sheng *et al*. 2020) gradient achieved strong electromagnetic absorption through strong hysteresis loss and dielectric loss (Sheng *et al*. 2020). Strong hysteresis loss was the main electromagnetic wave loss mode.

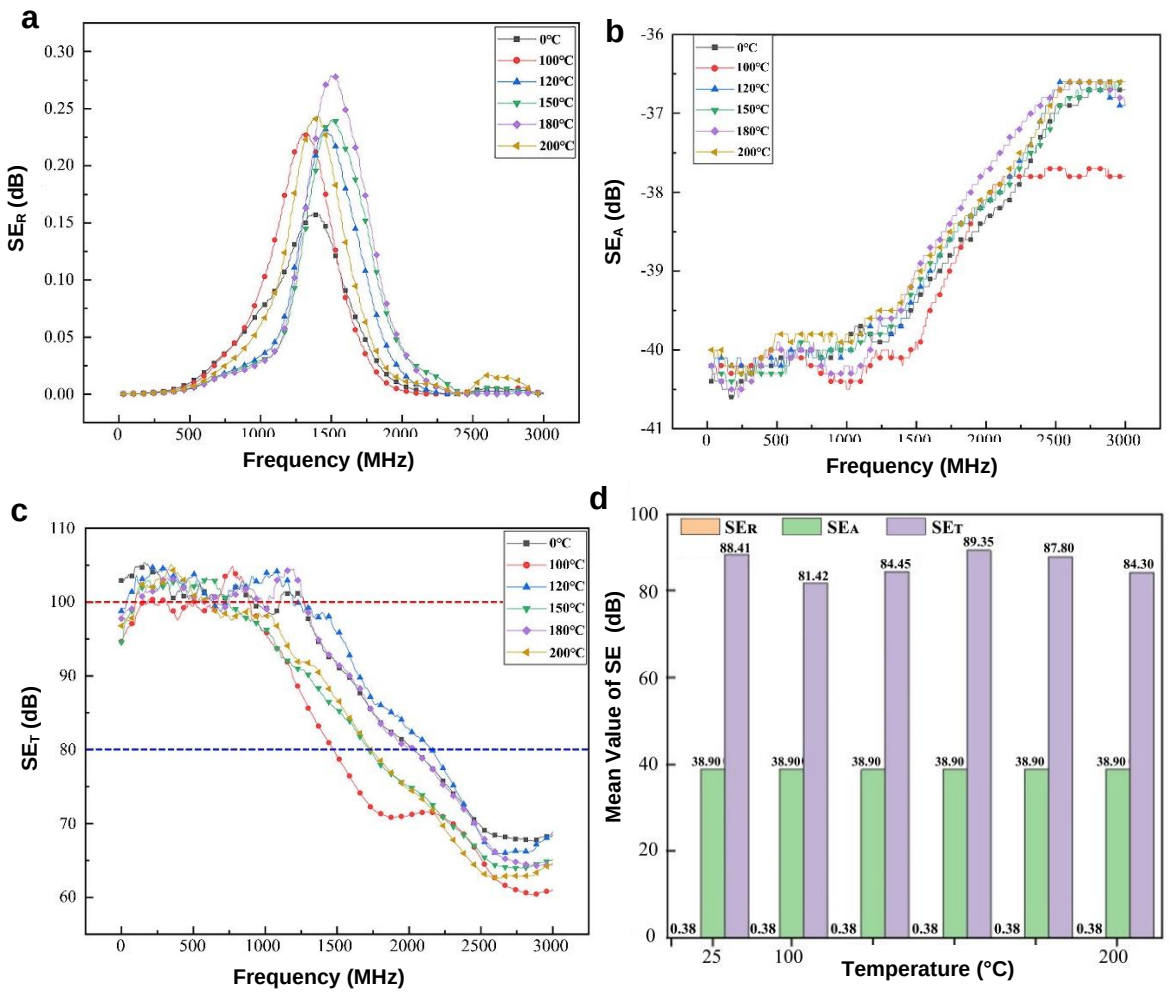

Fig. 14. Electromagnetic shielding effectiveness of electroless 2Cu1Ni composite before heat treatment (a: Reflection efficiency; b: Absorption efficiency; c: Electromagnetic shielding effectiveness; d: The average value)

Wood-based electroless Cu-Ni composites are known to have a synergistic effect on electromagnetic shielding effectiveness, and the main mechanism is the separation of conductive network and specific interface polarization mechanism of composite coatings (Tao *et al*. 2016; Ha *et al*. 2019). The ideal conductive network of the composite coatings showed superior charge storage capacity, and the polarization of the electric field promoted the absorption of more incident electromagnetic microwave energy (Yousefi *et al* 2014; Tao *et al*. 2016; Ha *et al*. 2019; Shen *et al*. 2020). With the change of heat treatment temperature, the thickness of the coating was also greatly improved. When the wood was treated *via* electroless 2Cu1Ni at 120 °C heat treatment, the coating thickness was 97.5 μm (Table 3).

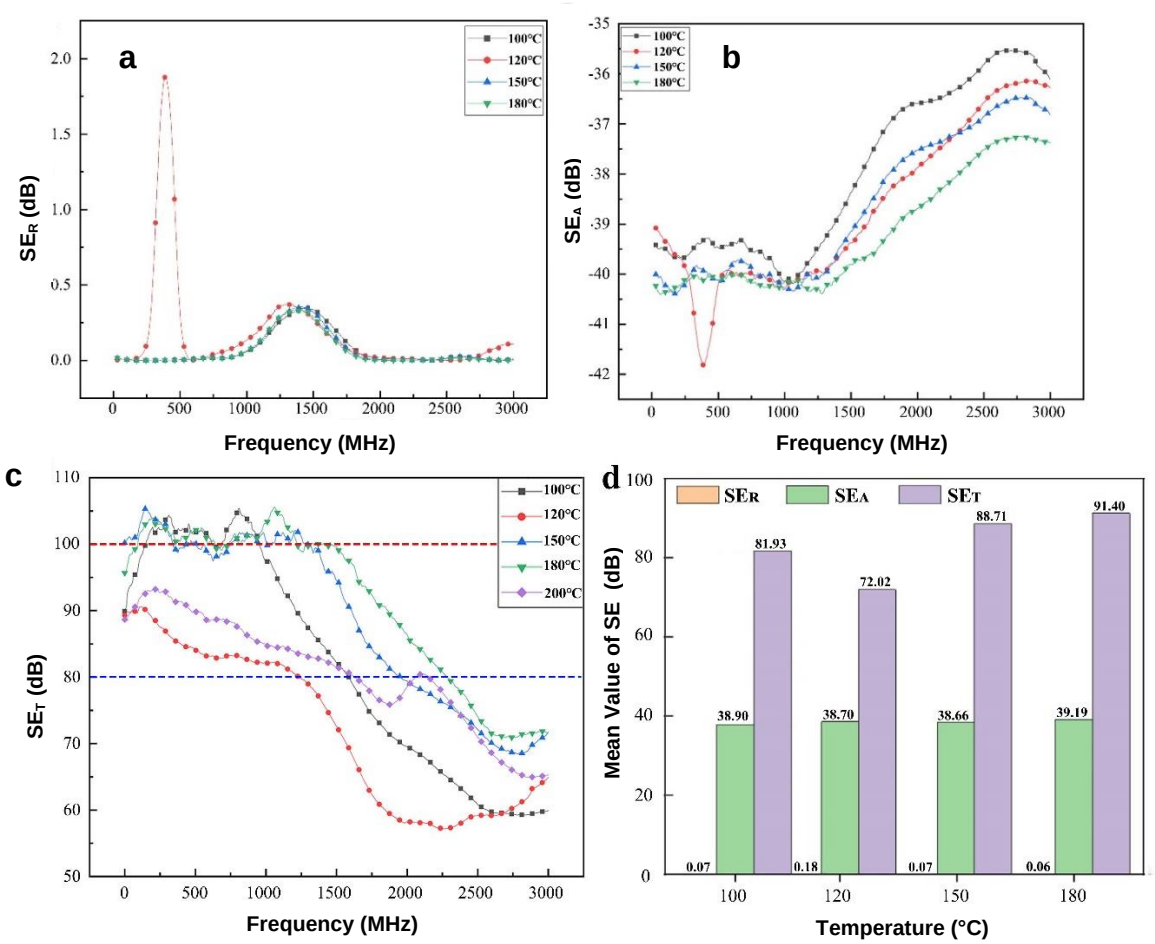

Fig. 15. Electromagnetic shielding effectiveness of electroless 2Cu1Ni composite after heat treatment (a: Reflection efficiency; b: Absorption efficiency; c: Electromagnetic shielding effectiveness; d: The average value)

Table 5. Relationship between Heat Treatment and Electromagnetic Shielding Effect

Temperature (°C)	Electromagnetic Shielding Effect (SE_T)/(dB)	
	Before Heat Treatment	After Heat Treatment
25	88.41	88.41
100	81.92	81.93
120	84.45	72.02
150	89.35	88.71
180	87.80	91.40
200	84.30	89.74

Due to the increase of the coating thickness and the shrinkage or disappearance of the pore structure, it was difficult for the incident electromagnetic wave to pass through the composite. Because the conductivity gradient structure of the composite material could

realize multi-medium interface loss and multiple reflection loss, the electromagnetic shielding effectiveness of the composite material was greatly improved, and the incident electromagnetic wave could be shielded efficiently.

The Mechanism of Electromagnetic Shielding Effectiveness

Figure 16 shows a schematic diagram of the electromagnetic shielding mechanism of wood matrix composites with electromagnetic gradient structure. Microscopically, wood has a micro/nano multi-scale pore structure, and its natural skeleton morphology could be used as a matrix template for other materials (Pan *et al*. 2022). However, the pores of the wood material restrict its application range, so it was of great importance to improve its performance by modification. Heat treatment was found to be an important wood modification technology. As shown in Fig. 7, the particles began to diffuse and tended to be flattened after heat treatment. The surface protrusions became smaller and disappeared. Before heat treatment, the Cu element and Ni elements added in the electroless solution preferentially adsorbed on the defects of the wood surface, which greatly reduced the surface energy. The treatment promoted the adsorption of metal coordination compound ions and reducing agent ions on the metal surface (Wang *et al*. 2020), and provided catalytic activity for the nucleation of the later alloy, which greatly improved its nucleation degree and deposition rate. From Fig. 16, it could be seen that the initial state of the metal coating's metal arrangement was more disordered between the metal and there were voids. Taking the composite coatings as the object, the effects of different heat treatment temperatures on the structure, conductivity, surface roughness, and morphology of the coatings were studied to improve the electromagnetic shielding effectiveness of wood-based composites with electromagnetic gradient structure. Studies had shown that with increased heat treatment temperature, composite coatings gradually transformed into a crystalline structure (Jia and Gao 2019), and the pore structure was improved. The wood-based composite coatings surface-treated *via* heat treatment were smoother, denser, and finer than that of the composite coatings without temperature treatment, and the surface roughness of the metal coatings on the wood surface could be up to 11.0 μm. A smaller particle size of Cu and Ni resulted in denser coatings (Liu *et al*. 2017).

The wood surface was treated twice with electroless Cu and once with electroless Ni, then treated with different temperature gradients to improve the morphology, roughness, conductivity, and hydrophobicity of the composite coatings to prepare the electromagnetic gradient structure with ideal electromagnetic shielding effectiveness. Firstly, the reason for high electromagnetic shielding efficiency was that the polarization mode in the process of microwave dielectric loss was dominated by interfacial polarization (Liu *et al*. 2016). The electromagnetic wave passed through the wood-based composites, and a large number of free charges spontaneously accumulated in the heterojunction surface between the metal Cu coatings, the metal Ni coatings, and the Cu coatings, the metal Ni coatings and the metal Ni coatings and the wood, resulting in the macroscopic dipole moment and Debye relaxation, thus accelerating the attenuation of electromagnetic wave and realizing the multi-media interface loss (Li *et al*. 2019). Secondly, the conductivity loss was undoubtedly another important factor. A better conductivity of the material resulted in a better electromagnetic shielding effect.

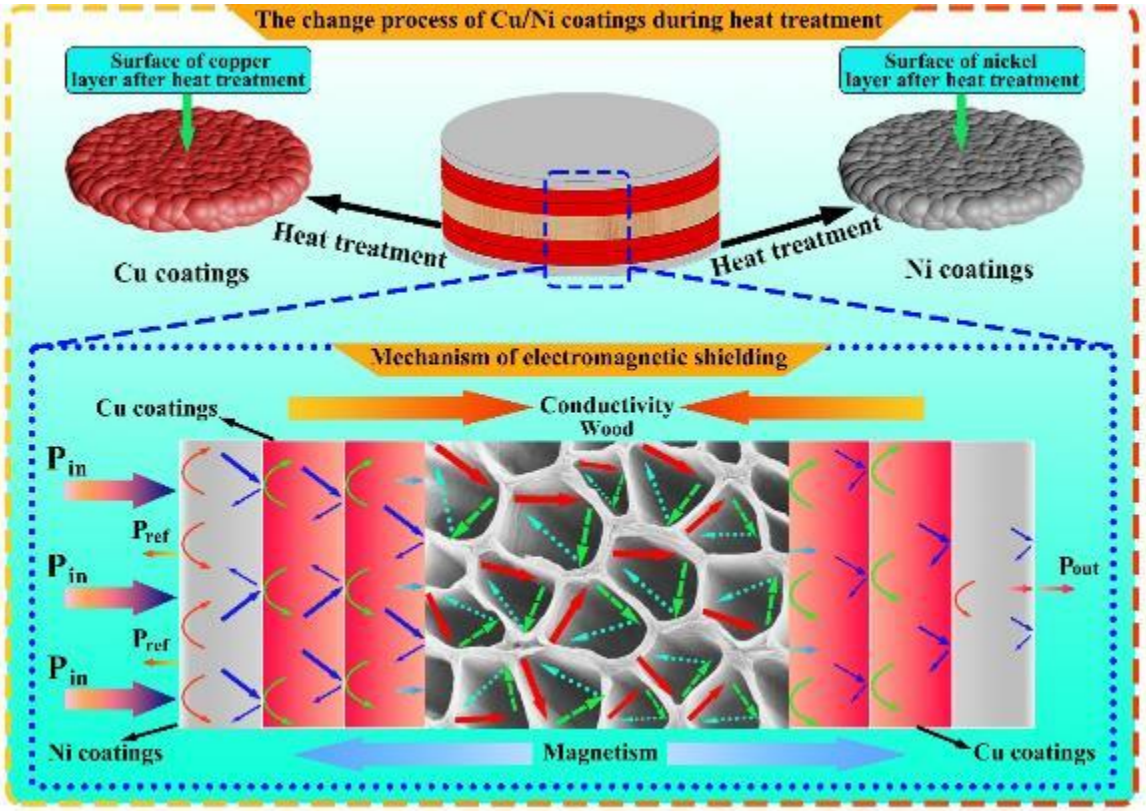

Fig. 16. Diagram of electromagnetic shielding mechanism of wood-based composites

In this study, the conductive network structure of the coatings was improved through heat treatment. The heat treatment accelerated the rearrangement of metal Cu and Ni particles and optimized surface structure. A perfect conductive structure was formed on the wood surface, and the good conductivity of the composite accelerated the efficiency of electromagnetic energy into heat energy (Yousefi *et al*. 2014; Liu *et al*. 2016; Tao *et al*. 2016; Liu *et al*. 2017; Wang *et al*. 2018, 2019; Ha *et al*. 2019; Jia *et al*. 2019; Li *et al*. 2019; Sheng *et al*. 2022). In addition, the gradient structure design would cause the electromagnetic shielding mechanism of absorption-reflection-reabsorption (Xu *et al*. 2018; Xu *et al*. 2020), which could noticeably attenuate the backward scattering of electromagnetic waves (Chen *et al*. 2011; Liu *et al*. 2017), so that the shielding effect was better. At the same time, the cross-section showed bright white in Fig. 11, which further illustrated that metal Cu and Ni particles would enter the wood pores. The heat treatment could accelerate metal Cu and Ni particles rearrangement, and ideal pore structure could be obtained. The high-density uniform microporous structure of wood-based composites provided more efficient air-wood interface, which played a decisive role in impedance mismatch and multiple internal reflection. The intrinsic permeable channel design of wood would shape slender metal and the conductive network structure was constructed, which could realize various reflection loss of electromagnetic wave.

CONCLUSIONS

1. The wood surface gradually flattened. A surface roughness of the metal coating on the wood surface of 11.0 μm was achieved.
2. When the wood was modified with electroless 2Cu1Ni *via* 120 °C heat treatment, the coating thickness was 97.5 μm. The interfacial morphology of the composite material verified that the surface and interface morphology of the composite coating was better at 120 °C.
3. The electrical conductivity increased with the increased temperature as well as with the extension of constant temperature treatment time.
4. When the wood material was plated with 2Cu1Ni and heat treated at 100 ℃, the contact angle of the composite was able to reach 119°.
5. The high-density uniform microporous structure of wood-based composites provided more efficient air-wood interface, which played a decisive role in impedance mismatch and multiple internal reflection. The average electromagnetic shielding efficiency of composite materials *via* electroless 2Cu1Ni with 180 ℃ heat treatment reached 91.4 dB ranging from 300 KHz to 3.0 GHz, which verified that the composite materials can shield 99.99% of the incident electromagnetic wave.

ACKNOWLEDGMENT

This work was supported by Natural Science Foundation of Inner Mongolia Autonomous Region (2022MS03006), The undergraduate innovation and entrepreneurship training program (Grant Nos. 202210129007, 202210129012, 202210129033, 202210129060, and 202110129007), the Start-up Project of Inner Mongolia Agricultural University High-level Talents Introduction Scientific Research (NDYB2016-24), The Colleges and Universities Science Research Project of Inner Mongolia Autonomous Region (NJZY18058 and NJZY21468), Science research innovation projects of the Inner Mongolia Agricultural University for undergraduate (KJCX2020025), and Science and Technology Innovation Leading Project of Inner Mongolia Autonomous Region (KCBJ2018013).

REFERENCES CITED

Abbasi, H., Antunes, M., and Velasco, J. I. (2019). "Recent advances in carbon-based polymer nanocomposites for electromagnetic interference shielding," *Prog. Mater. Sci*. 103, 319-373. DOI: 10.1016/j.pmatsci.2019.02.003

Chen, M. X., Zhu, Y., and Pan, Y. B. (2011). "Gradient multilayer structural design of CNTs/SiO_2 composites for improving microwave absorbing properties," *Mater. Des.* 32(5), 3013-3016. DOI: 10.1016/j.matdes.2010.12.043

Chen, Z. P., Xu, C., Ma, C. Q., Ren, W., and Cheng, H. M. (2013). "Lightweight and flexible graphene foam composites for high-performance electromagnetic interference shielding," *Adv. Mater.* 25(9), 1296-1300. DOI: 10.1002/adma.201204196

Fang, M. (2019). Establishment and Optimization of Thermal-mass Coupling Model for Wood Heat Treatment Kiln, Northeast Forestry University, Harbin, China.

Gao, Y. L. (2019). *Study on the Changes and Its Mechanism of Moisture Adsorption and Absorption Properties of High Temperature Heat Treated Chinese Fir Wood*, China Academy of Forestry Sciences, Beijing, China.

Gan, W., Chen, C., Giroux, M., Zhong, G., Goyal, M. M., Wang, Y., Ping, W., Song, J., Xu, S., He, S., Jiao, M., Wang, C., and Hu, L. (2020). "Conductive wood for high-performance structural electromagnetic interference shielding," *Chem. Mater.* 32, 5280-5289. DOI: 10.1021/acs.chemmater.0c01507

Hao, D. (2021). *Study on Interfacial Bonding Properties of Heat Treatment Glued Wood*, Nanjing Forestry University, Nanjing, China.

Ha, J. H., Hong, S. K., and Ryu, J. K. (2019). "Development of multi-functional graphene polymer composites having electromagnetic interference shielding and de-icing properties," *Polymers* 11(12), 2101. DOI: 10.3390/polym11122101

Hu, H. H., Li, Y. X., Gao, T., Yan, S. Y., Wu, S. T., Bandaru, S., Zheng, Y., Qin, G. W., and Zhang, X. F. (2021). "Sulfur-doped wood-derived porous carbon for optimizing electromagnetic response performance," *Nanoscale* 13(38), 16084-16093. DOI: 10.1039/D1NR04232G

Jia, Q. H., and Gao, D. (2019). "Effect of heat treatment on properties of electroless Ni-P coatings on magnesium alloy," *Ordnance Material Science and Engineering* 42 (6), 34-37. DOI:10.14024/j.cnki.1004-244x.20190924.001

Jia, X. C., Shen, B., Chen, J. L., Wang, G. Q., Sun, Z. P., and Zheng, W. G. (2022). "Multifunctional TPU composite foams with embedded biomass-derived carbon networks for electromagnetic interference shielding," *Compos. Commun*. 30, article no. 101062 DOI: 10.1016/j.coco.2022.101062

Li, Y., Liu, X. F., and Nie, X. Y. (2019). "Multifunctional organic-inorganic hybrid aerogel for self-cleaning, heat-insulating, and highly efficient microwave absorbing material," *Adv. Funct. Mater*. 29(10), 1807624. DOI: 10.1002/adfm.201807624

Liang, C., Qiu, H., Song, P., Shi, X., Kong, J., and Gu, J. (2020). "Ultra-light MXene aerogel/wood-derived porous carbon composites with walllike 'mortar/brick' structures for electromagnetic interference shielding," *Sci. Bull*. 65(8), 616-622. DOI: 10.1016/j.scib.2020.02.009

Lin, X. (2021). *Study on Polyethylene Glycol Modified Heat Treated Rubber Wood and its Properties*, Northeast Forestry University, Harbin, China.

Liu, P., Chen, D. F., and He, W. J. (2017). "Effects of Al_2O_3 particle size and heat treatment on the properties of Ni/Al_2O_3 composite coatings," *Surface Technology* 46(11), 230-236. DOI: 10.16490/j.cnki.issn.1001-3660.2017.11.031

Liu, Q. H., Cao, Q., and Bi, H. (2016). "CoNi@SiO_2@TiO_2 and CoNi@Air@TiO_2 microspheres with strong wideband microwave absorption," *Adv. Mater*. 28(3), 486-490. DOI: 10.1002/adma.201503149

Liu, J., Zhang, H. B., and Sun, R. (2017). "Hydrophobic, flexible, and lightweight MXene foams for high-performance electromagnetic-interference shielding," *Adv. Mater.* 29(38), 1702367. DOI: 10.1002/adma.201702367

Lou, Z., Wang, Q., Sun, W., Liu, J., Yan, H., Han, H., Bian, H., and Li, Y. (2021). "Regulating lignin content to obtain excellent bamboo-derived electromagnetic wave absorber with thermal stability," *Chem. Eng. J.* 430(10), article no. 133178. DOI: 10.1016/j.cej.2021.133178

Ma, Y. Y. (2019). *Study on Surface Plasma Treatment of High Temperature Heat Treatment Wood*, Fujian Agriculture and Forestry University, Fuzhou, China.

Meng, F. B., Wang, H. G., Huang, F., Guo, Y. F., Wang, Z. Y., Hui, D., and Zhou, Z. W. (2018). "Graphene-based microwave absorbing composites: A review and prospective," *Compos. B- Eng*. 137, 260-277. DOI: 10.1016/j.compositesb.2017.11.023

Pan, Y. F., Zhang, C. X., and Yu, H. B. (2020). "Hollow morphology, crystallization and phase transformation behavior of magnetic hollow composite materials based lignocellulose fibers via heat treatment," *Vacuum* 178, 109389. DOI: 10.1016/j.vacuum.2020.109389

Pan, Y. F., Guo, Q., and Yin, D. W. (2022). "Micro-nanoarchitectonics of electroless Cu/Ni composite materials based on wood," *J. Inorg. Organomet. Polym. Mater*. 32(2), 687-699. DOI: 10.1007/s10904-021-02155-2

Qi, F. Q., Wang, L., Zhang, Y. L., Ma, Z. L., Qiu, H., and Gu, J. W. (2021). "Robust Ti3C2Tx MXene/starch derived carbon foam composites for superior EMI shielding and thermal insulation," *Mater. Today Phys.* 21, article no. 100512. DOI: 10.1016/j.mtphys.2021.100512

Sheng, A., Ren, W., and Yang, Y. Q. (2020). "Multilayer WPU conductive composites with controllable electro-magnetic gradient for absorption-dominated electromagnetic interference shielding," *Compos. Part A- Appl. S.* 129, article no. 105692. DOI: 10.1016/j.compositesa.2019.105692

Shen, Z. M., and Feng, J. C. (2019). "Preparation of thermally conductive polymer composites with good electromagnetic interference shielding efficiency based on natural wood-derived carbon scaffolds," *ACS Sustainable Chem. Eng*. 7(6), 6259-6266. DOI: 10.1021/acssuschemeng.8b06661

Srivastava, S. K., and Manna, K. (2022). "Recent advancements in the electromagnetic interference shielding performance of nanostructured materials and their nanocomposites: A review," *J. Mater. Chem. A*. 10(14), 7431-7496. DOI: 10.1039/D1TA09522F

Sun, J., Wang, L., and Hu, K. (2015). "Fabrication of superhydrophobic surfaces on copper substrates via flow plating technology," *Micro Nano Lett*. 10(2), 88-92. DOI: 10.1049/mnl.2014.0440

Tao, Y. B., Li, P., and Shi, S. Q. (2016). "Effects of carbonization temperature and component ratio on electromagnetic interference shielding effectiveness of wood ceramics," *Materials* 9(7), 540. DOI: 10.3390/ma9070540

Thomassin, J. M., Jerome, C., and Huynen, I. (2013). "Polymer/carbon based composites as electromagnetic interference (EMI) shielding materials," *Mater. Sci. Eng. R Rep.* 74(7), 211-232. DOI: 10.1016/j.mser.2013.06.001

Wang, Y. X., Yang, H. M., and Xiao, M. H. (2018). "Effect of heat treatment temperature on properties of electroless composite Ni-P-CeO_2 coatings," *Hot Working Technology* 47(10), 204-207. DOI:10.14158/j.cnki.1001-3814.2018.10.053

Wang, Q. W., Zhang, H. B., and Liu, J. (2019). "Multifunctional and water-resistant mxene-decorated polyester textiles with outstanding electromagnetic interference shielding and joule heating performances," *Adv. Funct. Mater*. 29(7), article no. 1806819. DOI: 10.1002/adfm.201806819

Wang, Y., Wang, W., and Yu, D. (2020). "Multilayer-structured Ni-Co-Fe-P/polyaniline/ polyimide composite fabric for robust electromagnetic shielding with low reflection characteristic," *Chem. Eng. J.* 380(12), 108-113. DOI: 10.1016/j.cej.2019.122553

Xiao, Y. M., Sun, C. X., and Liu, J. K. (2020). "Research on the corrosion resistance of Cu/Ni composite bionic super-smooth surface," *Plating and Finishing* 42(1), 7-11. DOI: 10.3969/j.issn.1001-3849.2020.01.002

Xu, Y. D., Yang, Y. Q., and Yan, D. X. (2018). "Gradient structure design of flexible waterborne polyurethane conductive films for ultraefficient electromagnetic shielding with low reflection characteristic," *ACS Appl. Mater. Interfaces* 10(22), 19143-19152. DOI: 10.1021/acsami.8b05129

Xu, Y. L., Uddin, A., and Estevez, D. (2020). "Lightweight microwire/graphene/silicone rubber composites for efficient electromagnetic interference shielding and low microwave reflectivity," *Compos. Sci. Technol.* 189, article no. 108022. DOI: 10.1016/j.compscitech.2020.108022

Xiong, C. Y., Wang, T. X., Zhang, Y. K., Meng, Z., and Ni, Y. H. (2022). "Recent progress on green electromagnetic shielding materials based on macro wood and micro cellulose components from natural agricultural and forestry resources," *Nano Research* 15(8), 1-27. DOI: 10.1007/s12274-022-4512-2

Xiong, C. Y., Li, M. R., Han, Q., Zhao, W., Dai, L., and Ni, Y. H. (2022). "Screen printing fabricating patterned and customized full paper-based energy storage devices with excellent photothermal, self-healing, high energy density and good electromagnetic shielding performances," *Journal of Materials Science & Technology* 97, 190-200. DOI: 10.1016/j.jmst.2021.04.054

Yan, M. H. (2021). *Wood Properties and Dynamic Moisture Sorption of High-temperature Thermally Treated Larch gmelinii*, Northeast Forestry University, Harbin, China.

Yousefi, N., Sun, X. Y., and Kim, J. K. (2014). "Highly aligned graphene/polymer nanocomposites with excellent dielectric properties for high-performance electromagnetic interference shielding," *Adv. Mater*. 26(31), 5480-5487. DOI: 10.1002/adma.201305293

Yu, M. (2021). *Study on Temperature Field Uniformity and Control Method of Wood Carbonization Tank*, Northeast Forestry University, Harbin, China.

Yu, R., Zhang, H., and Guo, B. (2022). "Conductive biomaterials as bioactive wound dressing for wound healing and skin tissue engineering," *Nano-Micro Lett*. 14(1), 1-46. DOI: 10.1007/s40820-021-00751-y

Zhang, J., Qi, C. S., and Mu, J. (2020). "Effects of thermal treatment temperature and duration on mass loss and rupture modulus of *Cunninghamia lanceolata*," *Beijing Forestry University Journal* 42(10), 137-144. DOI:10.12171/j.1000-1522.20200257.

Zheng, Y., Song, Y. J., and Gao, T. (2020). "Lightweight and hydrophobic three-dimensional wood-derived anisotropic magnetic porous carbon for highly efficient electromagnetic interference shielding," *ACS Appl. Mater. Interfaces* 12(36), 40802-40814. DOI: 10.1021/acsami.0c11530

Article submitted: August 13, 2022; Peer review completed: October 1, 2022; Revised version received and accepted: October 9, 2022; Published: October 17, 2022.
DOI: 10.15376/biores.17.4.6718-6739